Nuclear Instruments and Methods in Physics Research B 328 (2014) 42–47

Contents lists available at ScienceDirect

Nuclear Instruments and Methods in Physics Research B

journal homepage: www.elsevier.com/locate/nimb

Molecular dynamics study on interfacial thermal conductance of unirradiated and irradiated SiC/C

Qingyu Wang [a,*], Chenglong Wang [a], Yue Zhang [b], Taosheng Li [c]

[a] College of Nuclear Science and Technology, Fundamental Science on Nuclear Safety and Simulation Technology Laboratory, Harbin Engineering University, Harbin 150001, China
[b] Nuclear and Radiation Safety Center, MEP, Beijing 100082, China
[c] Institute of Nuclear Energy Safety Technology, Chinese Academy of Sciences, P.O. Box 1126, Hefei 230031, China

ARTICLE INFO

Article history:
Received 6 February 2014
Received in revised form 26 February 2014
Accepted 1 March 2014
Available online 27 March 2014

Keywords:
Molecular dynamics
SiC composite
Interface
Thermal conductivity
Irradiation

ABSTRACT

SiC_f/SiC composite materials have been considered as candidate structural materials for several types of advanced nuclear reactors. Both experimental and computer simulations studies have revealed the degradation of thermal conductivity for this material after irradiation. The objective of this study is to investigate the effect of SiC/graphite interface structure and irradiation on the interfacial thermal conductance by using molecular dynamics simulation. Five SiC/graphite composite models were created with different interface structures, and irradiation was introduced near the interfaces. Thermal conductance was calculated by means of reverse-NEMD method. Results show that there is a positive correlation between the interfacial energy and interfacial C–Si bond quantity, and irradiated models showed higher interfacial energy compared with their unirradiated counterparts. Except the model with graphite atom plane parallel to the interface, the interfacial thermal conductance of unirradiated and irradiated (1000 eV) models, increases as the increase of interfacial energy, respectively. For all irradiated models, lattice defects are of importance in impacting the interfacial thermal conductance depending on the interface structure. For the model with graphite layer parallel to the interface, the interfacial thermal conductance increased after irradiation, for the other models the interfacial thermal conductance decreased. The vibrational density of states of atoms in the interfacial region was calculated to analyze the phonon mismatch at the interface.

1. Introduction

Continuous silicon carbide (SiC) fiber-reinforced SiC-matrix (SiC_f/SiC) composites have been considered as one of the most important candidate structural materials for nuclear reactors, such as light water reactor (LWR) [1], high-temperature gas-cooled reactor (HTGR) [2] and future fusion reactor [3], for their low radioactivity, high-temperature strength and chemical inertness, high radiation stability, low induced-activation and low after-heat properties [4,5]. But there are still numerous challenges such as their thermal conductivity, radiation stability, hermetic behavior and joining technology [6,7]. Many efforts have been made in these decades including extensive worldwide cooperation.

As we all know, the fiber/matrix interfaces play an important role in accommodating fiber-matrix load transfer, debond, and sliding. For most ceramic materials, SiC in particular, due to a relatively low density of valence electrons [8], the thermal transport across conductor (Graphite)/semiconductor (SiC) interface is primarily by interphonon transport [9]. But the interface phonon scattering, arising from the poor mechanical or chemical adherence between fiber and matrix, is the main mechanisms to create thermal resistance, "Kapitza-type", for heat conduction [10–12]. More important, interface thermal resistance has the huge negative influences on the thermal conductivity of the composites [13]. Therefore, if the interface thermal resistance is too high, it will lower the thermal conductivity of the composite components and degrade the heat removal and thermal stress reduction in fusion reactors.

It is difficult to study detailed thermal energy transport across these small scale interfaces through physical experiments, but molecular dynamics (MD) simulations offer the possibility to understand the detailed mechanisms of the interfacial transport phenomena [14]. There are two main approaches to analyze thermal transport through MD [15]: (1) equilibrium molecular dynamics (EMD) based approach that uses fluctuation dissipation theorem or the Green-Kubo method and (2) non-equilibrium molecular dynamics (NEMD) based approach that imposes a

* Corresponding author. Tel./fax: +86 451 82518884.
E-mail address: wangqingyu@hrbeu.edu.cn (Q. Wang).

http://dx.doi.org/10.1016/j.nimb.2014.03.004
0168-583X/

temperature gradient and subsequently measuring thermal conductivity using the classical Fourier law of thermal conduction. However, compared to EMD, NEMD is more suitable to study an inhomogeneous system, such as the interface studied here, because the Kapitza conductance, which is a local property, cannot be correctly treated under the assumption that the system is homogeneous [16]. In this work, reverse NEMD (rNEMD) is used. In rNEMD, the heat flux is imposed on the system by the unphysical velocity exchange, after reaching steady state, the energy exchange and heat flux is balanced in the opposite direction, and then the resulting temperature gradient is measured to calculate the thermal conductivity. The advantages and disadvantages of rNEMD have been discussed in detail elsewhere [17], and not to be repeated here.

In this paper, all work has been done by classical MD modeling of interfacial heat transport between SiC-fibre and pyrolytic carbon interphase (SiC/C). Five composite models with different crystal orientations were systematically studied; besides, effect of irradiation on the interfacial thermal conductance was also discussed.

2. Methodologies

Five SiC/C composite models were established and studied in this work, each model includes three parts and two SiC/C interfaces. On each side is single crystal 3C-SiC with a lattice spacing of 4.359 Å (named a_0). The middle part is graphite, with carbon atoms arranged in a honeycomb lattice, 1.42 Å separated in each layer, and 3.35 Å between planes. In order to ensure SiC and graphite to meet the periodic boundary condition (PBC) in all directions at the same time, there are only several specific angles and cross-section sizes that can satisfy the requirement. As shown in the top panel of Fig. 1, α is the angle between the graphite plane and SiC, which is 56.705°, thus this model is denoted as M56. The other four angles are 90.000°, 77.315°, 28.560° and 0.000° (denoted as M90, M77, M28, M0), respectively. The M0, $8a_0 \times 82a_0 \times 10a_0$, involves 29744 graphite atoms and 26720 SiC. The M28, M56, M77, $8a_0 \times 82a_0 \times 7a_0$, involve 21728, 21000, 21252 graphite atoms, respectively, and 9352 SiC each. The last one, M90, $8a_0 \times 82a_0 \times 9a_0$, involves 26624 graphite atoms and 11880 SiC.

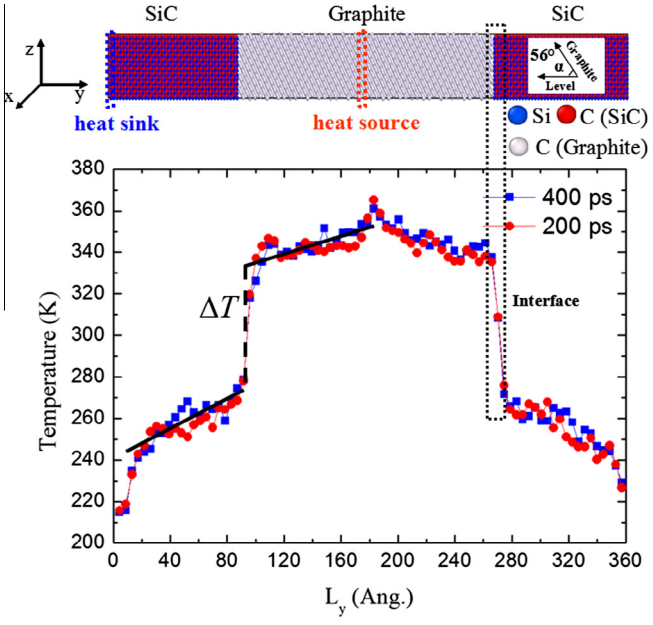

Fig. 1. (Top) Typical structure of SiC/C composite model. (Bottom) Temperature profile of SiC/C composite system. ΔT: temperature drop between SiC and graphite interface.

All MD simulations were performed using the LAMMPS package [18]. The SiC in each system was modeled using the modified analytical bond-order Tersoff-type potential (for thermal conductivity) [19] and hybrid Tersoff-ZBL potential (for irradiation) [20,21]. The graphite was modeled using the adaptive intermolecular reactive empirical bond order (AIREBO) potential [22]. The same potential was used for graphite-SiC interactions as in SiC. All initial molecular systems were equilibrated at a temperature of 300 K by NPH (constant number of particles, pressure, and enthalpy) ensemble and Langevin thermostat for 2 ns with a time step of 0.5 fs. After NPH relaxation, the systems were converted into NVE ensemble for calculating interface thermal conductance. In order to maintain the energy conserved, a value of 0.1 fs was chosen as the time step throughout the NVE simulations.

In order to impose a heat flux perpendicular to the interface, the system was divided into 82 slabs after the NPH relaxation, whose thickness was about 1 a_0, along the direction of heat flow. Slab 1 is defined as the "heat sink" and slab 42 as the "heat source". The constant heat flux (J_Q) was imposed through Müller-Plathe method [17]. As shown in the bottom panel of Fig. 1, the temperature profile does not change significantly from 200 to 400 ps, i.e., the systems had reached the steady-state. Also, the temperature drop near the interface (ΔT) was obtained from the temperature profile. The interfacial thermal conductance G can be obtained from the relationship [23]

$$G = J_Q/\Delta T \tag{1}$$

The interfacial energy E_{if} denotes the excess energy per unit interface area due to the existence of interface interaction as given by

$$E_{if} = \frac{1}{S_{interface}}(E - E_0) \tag{2}$$

where S is the total interface area, E and E_0 is the energy of the system with and without interface interaction, respectively.

The vibrational density of states (VDOS) denote the strength of phonons vibration mode in different frequency. It can be obtained from the fast Fourier transformation of the velocity autocorrelation function (VACF) [24].

$$\mathrm{VDOS}(\upsilon) = \int_{-\infty}^{\infty} \mathrm{VACF}(t) e^{-2\pi i \upsilon t} dt \tag{3}$$

where υ is the phonon frequency, t is the correlation time of VACF(t).

The systems equilibrated by NPH ensemble were used for the irradiation simulations. In order to ensure the system was sufficiently large to contain the cascades within the box and near the interface, the primary-knock-on atom (PKA), an energetic Si in the interface, was given a small kinetic energy of 250 or 500 eV projected through the interface between SiC and graphite. After irradiation, all the models were used for calculating the interfacial thermal conductance by the same method as above.

3. Results and discussion

3.1. Interfacial thermal conductance

The typical temperature profile of the SiC/C composite system with two interfaces is shown in the bottom panel of Fig. 1. As can be seen, there is no significant difference between 200 and 400 ps temperature profile, i.e., the whole system had reached the equilibrium state after 200 ps. By extrapolating to infinite length, an approach proposed by Schelling et al [15], the thermal

conductivity of bulk SiC and graphite (heat flow along the basal plane) are obtained to be 163 and 322 W/mK at 300 K by using the same procedure, respectively, comparable with their experimental values, 314 W/mK [25] and 250–500 W/mK [26] for single crystal β-SiC and pyrolytic graphite, respectively. Since the thermal conductivity of graphite is larger than that of SiC, the slop in graphite is lower as compared to SiC. The temperature of heat source and heat sink maintained at ~365 and ~215 K, respectively. There is an obvious temperature drop at the interfacial region due to the interface thermal resistance.

Fig. 2 exhibits the relationship between the interfacial energy and the interfacial graphite–Si bond density with and without irradiation. The bond length is 2.61 Å according to the Tersoff potential [20]. It is obvious that as the increase of interfacial C–Si bond density, the interfacial energy increases. Irradiated models show higher interfacial energy compared with their unirradiated counterparts.

The interfacial thermal conductance of all models are showed in Fig. 3. The Kapitza conductance of graphene with the length of 25 nm is 2393, 1764 and 1642 MW/m^{2}K for the grain orientation angle of 5.48°, 13.2° and 21.7° [27], which is comparable with the M0, M28 and M56 models. The calculated grain boundary thermal resistance of SiC is about $\sim 1 \times 10^{-10}$ m^{2}K/W to $\sim 7 \times 10^{-10}$ m^{2}K/W, corresponding to 2°–30° tilt angle [28]. Therefore the grain boundary thermal conductance of both of the two materials is of the same order as the composite models results in this work. As reported in Ref. [29], with Tyranno SA™ fiber and CVI matrix, the typical thermal conductivity of SiC/SiC composite is about 30–40 W/mK, corresponding to fiber/matrix interfacial thermal conductance, h, in the range of 100–1000 MW/m^{2}K, which is lower than the present results.

Also we can see that with the special structure the interfacial thermal conductance of both irradiated and unirradiated M90 is an order of magnitude lower than that of others. And among unirradiated and irradiated (1000 eV) M0, M28, M56 and M77, the interfacial thermal conductance increases as the interfacial energy increases. As has been reported in Ref. [30], there is a positive correlation between interfacial energy and interfacial thermal conductance. According to this, with the higher interfacial energy, irradiated models should have higher interfacial thermal conductance compared with their unirradiated counterparts. But in contrast, all of the interfacial thermal conductance decrease after irradiation except M90. This suggests that interfacial thermal conductance depends not only on the interfacial energy but also the defects induced by irradiation. This is also evidenced by the results

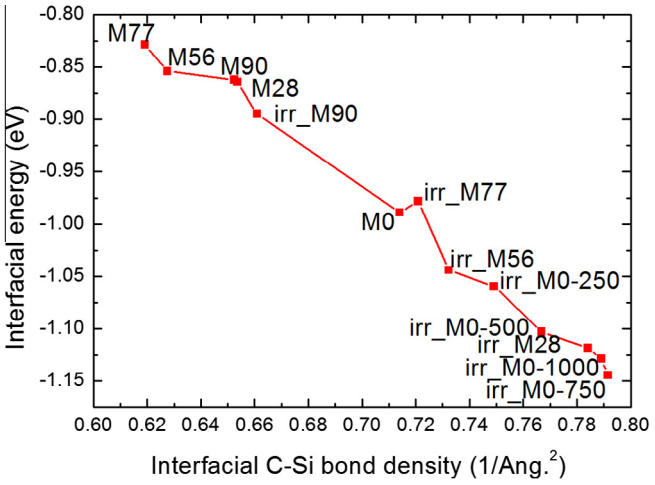

Fig. 2. Interfacial energy as a function of interfacial C(Graphite)–Si bond density.

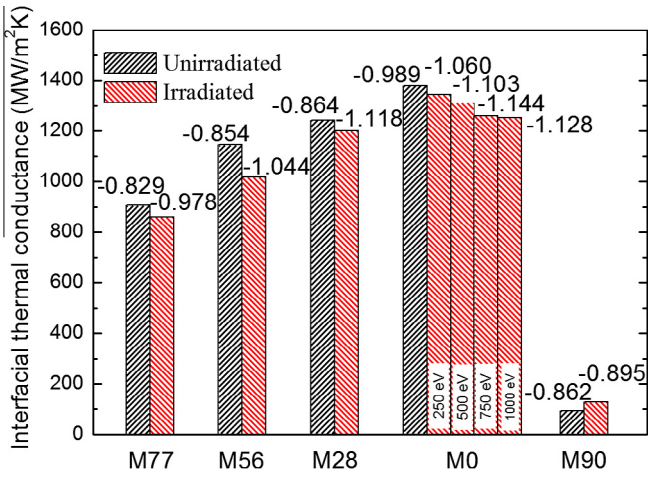

Fig. 3. Effect of interfacial energy on interfacial thermal conductance, the numbers on top of the bars represent the interfacial energy (eV).

of M0, which show that the interfacial thermal conductance decreases with increasing irradiation doses. The detailed mechanisms will be discussed in Section 3.3.

3.2. Mechanisms behind the near-interface thermal conductance

In order to qualitatively explain why the interfacial thermal conductance of M0, M28, M56 and M77 decrease and that of M90 increases after irradiation, the vibrational properties of atoms in the interfacial region are analyzed. Note that in this case the interfacial region atom chain is composed of ...C–Si–C–Si–graphite–graphite..., where the 1st Si atoms adjacent to the 1st Graphite atoms are interface. Every graphite layer used to calculate VDOS is separated by 1–1.5 Å, roughly equal to the spacing between Si and C layer, except M90. In M90, the graphite layer spacing is about 3.35 Å. Due to the non-uniform defects distribution induced by irradiation, all atoms in the layer are selected to calculate their VDOS via Fourier transformation of the atomic velocity autocorrelation function.

Fig. 4 exhibits the irradiated and unirradiated temperature profiles of M0 (a) and M90 (b). As has been reported, e.g., in Ref. [24], the largest temperature drop does not take place at the interface, the same phenomenon can be observed from Fig. 4 for both M0 and M90. Fig. 5 shows the VDOS of 1st Si, 5th Si, 1st C, 5th C, 1st Graphite and 5th Graphite of unirradiated M0, representing interface and non-interface atom layers, respectively. For the 1st SiC and 1st Graphite atoms, the medium-frequency (20–25, 33–40 THz) phonon modes are all enhanced compared with 5th atom layers and at the same time the low-frequency (6–18 THz) are reduced, which accounts for the strong coupling between 1st C, 1st Si and 1st Graphite. This effect enhanced the interfacial heat transfer, so there is not a large temperature drop at the interface as can be seen in Fig. 4. And similar phenomenon was also observed in other models.

However, at the same time, there are clear differences between the temperature profiles of M0 and M90, that the largest temperature drop in M0 takes place between 1st SiC and 2nd SiC and in M90 the drop takes place between 1st Graphite and 2nd Graphite as can be seen in Fig. 4. Fig. 6 shows the VDOS of graphite, C and Si in unirradiated M0 and M90 models. In Fig. 6(b), for the 1st C atom layer in M0, the high-frequency (~30 THz) peak shifts a bit to the left and splits into several peaks, and also for the 2nd C atom layer, the medium-frequency (23–26 THz) phonon modes are enhanced. In Fig. 6(c), for both 1st Si and 2nd Si atom layers, the high-frequency (30 THz) and low-frequency (9–18 THz) peaks are all

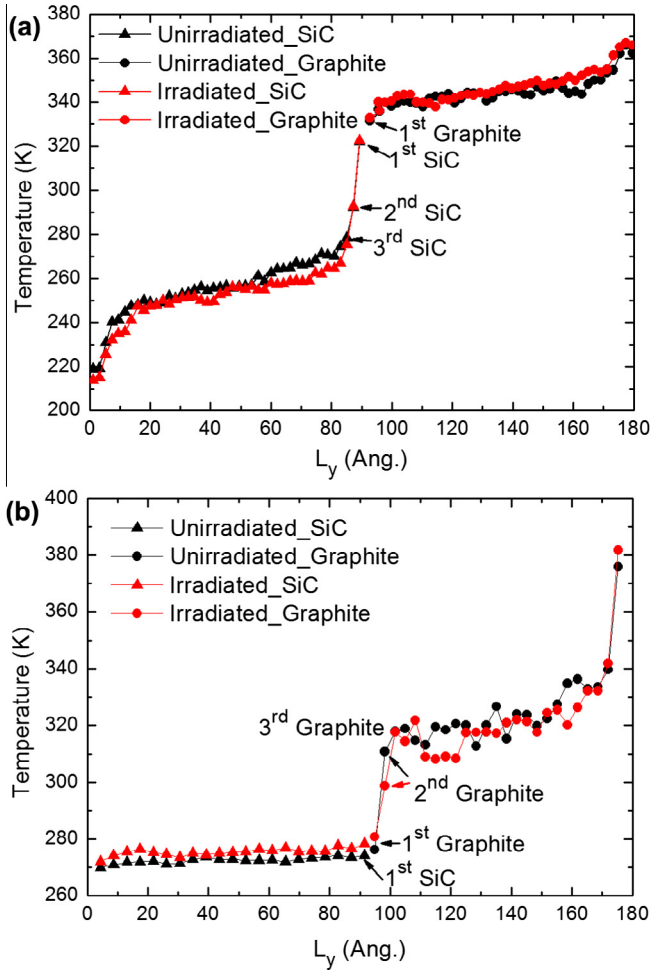

Fig. 4. Temperature profiles of unirradiated and irradiated M0 (a) and M90 (b).

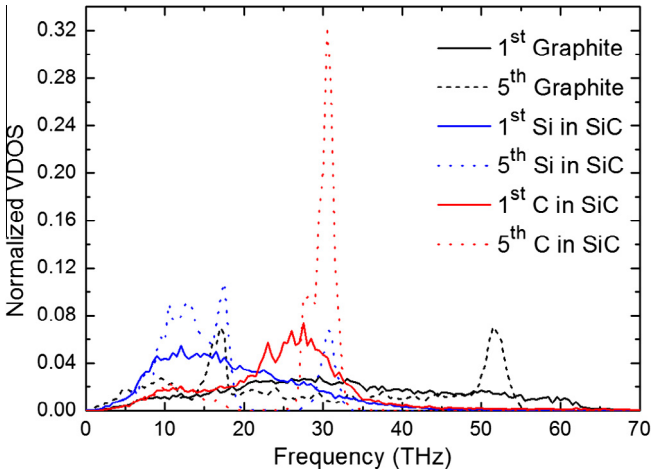

Fig. 5. Comparison of VDOS of atoms in the interface region and bulk of unirradiated M0.

reduced, and the medium-frequency (20–28 THz) phonon modes are enhanced. All of these leads to large VDOS mismatch between the 1st SiC, 2nd SiC and inner bulk SiC, which is the main reason for the large temperature drop in SiC region [24,31]. Maybe because of the very high thermal conductivity (1840 W/mK at 300 K) of graphite along the layer, although the low-frequency (10 and 17 THz) peaks and the high-frequency (52 THz) peak are all reduced (Fig. 6(a)), the slop in graphite interfacial region is slightly larger as compared to that in bulk graphite, there is not an obvious temperature drop in graphite area.

Fig. 6(d–f) show the VDOS of graphite, C and Si of unirradiated M90 model, respectively. It can be seen that for 1st Graphite atoms, the low-frequency (0 and 0.5 THz) phonon modes disappeared, the low-frequency (10 and 17 THz) and the high-frequency (52 THz) peaks are all reduced, and the medium-frequency (20–32 THz) phonon modes are enhanced, all of these leads to the large VDOS mismatch between 1st Graphite and other graphite, which is mainly responsible for the large temperature drop at the graphite region. In Fig. 6(e and f), there are still large VDOS mismatch between 1st SiC and bulk SiC. For the graphite layers in M90 are parallel to the interface and perpendicular to the heat flow, and the low interlamination thermal conductivity (8.58 W/mK at 300 K) of graphite, the heat flux applied to M90 is only 3.3 GW/m^2 (100 GW/m^2 in M0), resulting in the large temperature drop in the near-interface graphite and the large slop in graphite.

3.3. Mechanisms behind the thermal conductance change after irradiation

Fig. 7(a–c) show the VDOS of graphite, C and Si in irradiated M0. In Fig. 7(b), for the 2nd C, 3rd C, 4th C and 5th C atoms, the medium-frequency (24–26 THz) phonon modes are enhanced compared to the unirradiated models as shown in Fig. 6(b). And in Fig. 7(c), for the first 3 Si atom layers, the medium-frequency (20–27 THz) are enhanced as compared to the unirradiated models as shown in Fig. 6(c). This is due to additional phonon scattering caused by irradiation-induced defects, which leads to VDOS mismatch between the interfacial region and bulk SiC. And in Fig. 4(a), there is an obvious temperature drop between 3rd SiC and 4th SiC, which makes the thermal conductance decrease. With the increase of irradiation does, the point defect concentration increase, the VDOS mismatch between the interfacial region and bulk SiC increase as well, therefore the thermal conductance decrease. That is the main reason for the decrease of interfacial thermal conductance of M0, as the does increase.

Fig. 7(d–f) show the VDOS of graphite, C and Si in irradiated M90. From Fig. 7(d), for 1st Graphite atoms, the high-frequency (54–57 THz) and medium-frequency (19–24 THz) peaks are all reduced, and the low-frequency (14–17 THz) phonon modes are enhanced, which leads to relatively small VDOS mismatch between the interfacial region and bulk graphite. So from Fig. 4(b), the temperature drop between 1st Graphite and 2nd Graphite becomes smaller, although the drop between 2nd Graphite and 3rd Graphite becomes bigger, generally, the whole drop becomes smaller, and the interfacial thermal conductance increased.

In general, with the increase of interfacial energy, the interfacial thermal conductance should increase, too. In this article, the irradiated models have shown higher interfacial energy compared with their unirradiated counterparts. But in fact, all the interfacial thermal conductance decrease after irradiation except M90, i.e., irradiation has an effect on interfacial thermal conductance. It is worthy to point out that early studies by Katoh [32,33] have shown that the thermal conductivity of post-irradiated SiC/SiC composites obviously decreased at room temperature. As has been reported, e.g., in Refs. [8,31,32], due to the additional phonon scattering caused by the mismatch of phonon spectrum arose from the accumulation of lattice point defects and clusters of various types, the irradiated crystalline SiC showed thermal conductance degradation. All the irradiation-induced vacancies, self-interstitials, antisites, and their clusters are considered to have negative effects on thermal conductance. But up to now, there are still some difficulties to explain the thermal conductance degradation quantitatively by different defect species [34,35]. Crocombette [36] points

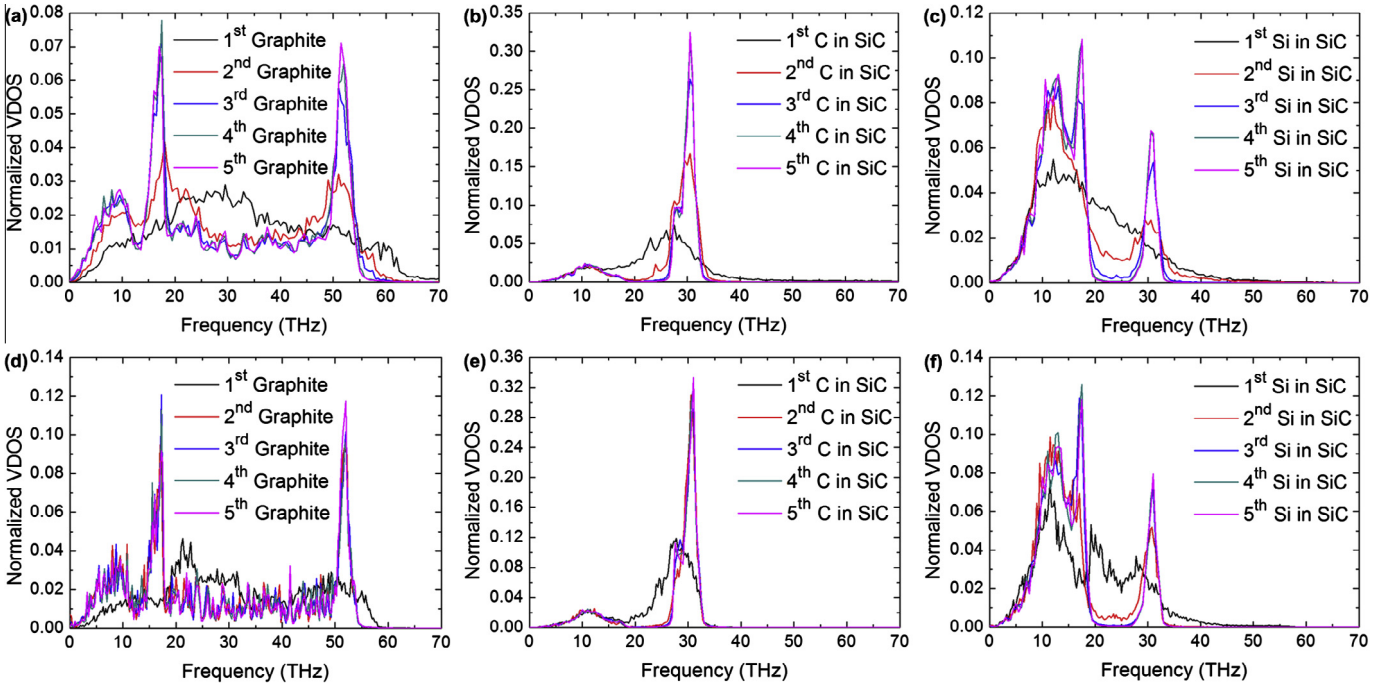

Fig. 6. Comparison of VDOS of atoms in unirradiated M0 (a, b and c) and M90 (d, e and f).

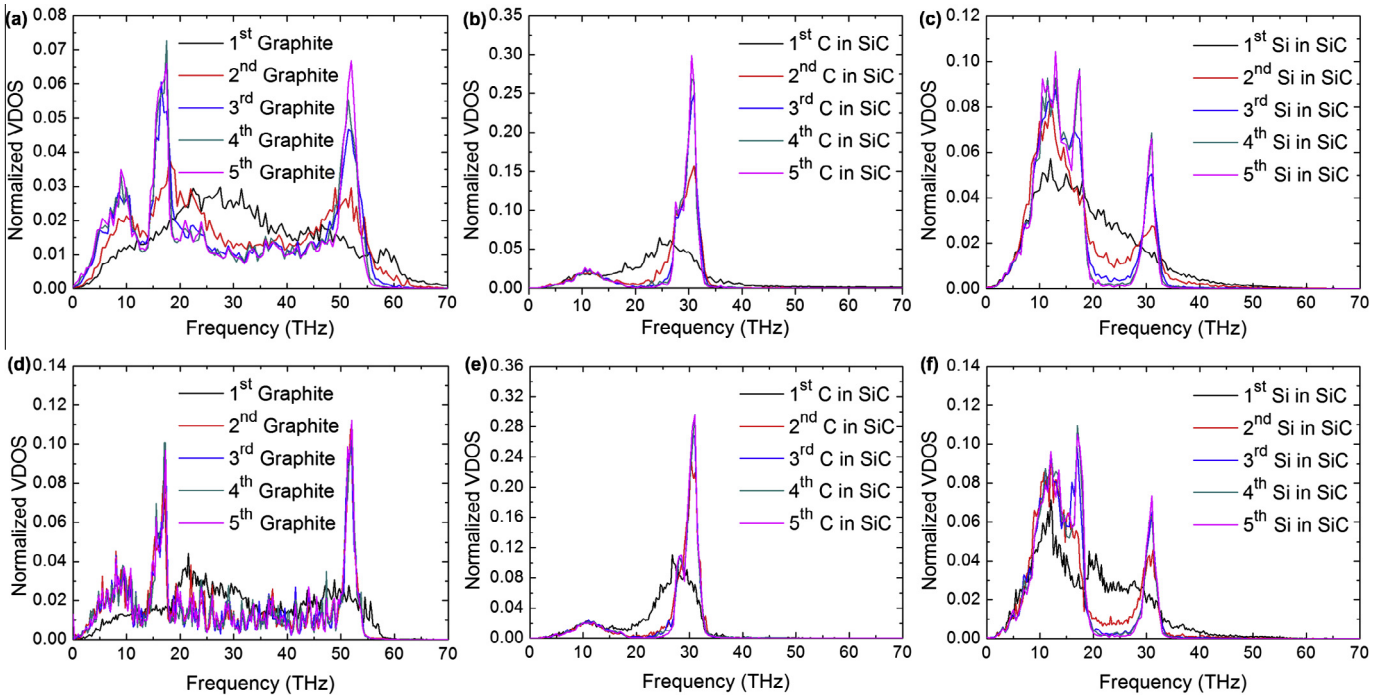

Fig. 7. Comparison of VDOS of atoms in irradiated M0 (a, b and c) and M90 (d, e and f).

out that the thermal resistivity due to a population of a given type of point defects in an insulating material is proportional to their concentration up to very large concentrations. Bockstedte [37] and Kaoth [38] point that there are high concentrations of vacancies and antisites in irradiated SiC, and these two types of defects are playing important role in their impact on the thermal conductance degradation. Ratsifaritana [39] points out that with the relatively small distortion, a vacancy cannot cause significant phonon scattering. Klemens [40] points out that with higher lattice strain, self-interstitials have significantly higher phonon scattering cross-section than vacancies. In this work, the irradiation defects cannot be neglected in the present time scale and played noticeable roles in impacting the interfacial thermal conductance.

4. Conclusion

The interfacial thermal conductance of unirradiated and irradiated SiC/C composites was studied using nonequilibrium molecu-

lar dynamics simulations. There is positive correlation between the interfacial energy and interfacial C-Si bond quantity, and irradiated models showed higher interfacial energy compared with their unirradiated counterparts. The interfacial thermal conductance of unirradiated and irradiated (1000 eV) M77, M56, M28 and M0, increases as the increase of interfacial energy, respectively. For irradiated models, lattice defects played an important role in impacting the interfacial thermal conductance. Except M90, the other models showed decreased interfacial thermal conductance after irradiation. With the special structure, the interfacial thermal conductance of both irradiated and unirradiated M90 is an order of magnitude lower than others. And different from the rest, the interfacial thermal conductance of M90 increases after irradiation.

Acknowledgement

The authors thank Lin Shao for his helpful idea and discussions. This work was supported by the Fundamental Research Funds for the Central Universities (Grant No. HEUCFT1103). We also acknowledge the High Performance Computing Center of Harbin Engineering University and Supercomputing Center of Chinese Academy of Sciences for providing computing resources.

References

[1] K. Yueh, D. Carpenter, H. Feinroth, Clad in clay, Nucl. Eng. Int. 55 (666) (2010) 14–16.
[2] L.L. Snead, Y. Katoh, W. Windes, K. Smit, Candidate structural materials for in-Core VHTR application, Trans.-Am. Nucl. Soc. 98 (2008) 1019.
[3] A.R. Raffray, R. Jones, G. Aiello, M. Billone, L. Giancarli, H. Golfier, A. Hasegawa, Y. Katoh, A. Kohyama, S. Nishio, B. Riccardi, M.S. Tillack, Design and material issues for high performance SiCf/SiC-based fusion power cores, Fusion Eng. Des. 55 (1) (2001) 55–95.
[4] A. Kohyama, S. Konishi, A. Kimura, Fusion materials and fusion engineering R & D in Japan, Nucl. Eng. Technol. 37 (5) (2005) 423.
[5] L.L. Snead, T. Nozawa, M. Ferraris, Y. Katoh, R. Shinavski, M. Sawan, Silicon carbide composites as fusion power reactor structural materials, J. Nucl. Mater. 417 (1) (2011) 330–339.
[6] H. Yu, X. Zhou, W. Zhang, H. Wang, S. Zhao, Z. Luo, Research and development of thermal conductivities of SiC/SiC composites for fusion applications, Mater. Rev. 3 (2010) 023.
[7] R.H. Jones, L. Giancarli, A. Hasegawa, Y. Katoh, A. Kohyama, B. Riccardi, W.J. Weber, Promise and challenges of SiCf/SiC composites for fusion energy applications, J. Nucl. Mater. 307 (2002) 1057–1072.
[8] L.L. Snead, T. Nozawa, Y. Katoh, T.S. Byun, S. Kondo, D.A. Petti, Handbook of SiC properties for fuel performance modeling, J. Nucl. Mater. 371 (1) (2007) 329–377.
[9] Z. Liang, H.L. Tsai, Reduction of solid–solid thermal boundary resistance by inserting an interlayer, Int. J. Heat Mass Transf. 55 (11) (2012) 2999–3007.
[10] Z. Tian, H. Hu, Y. Sun, A molecular dynamics study of effective thermal conductivity in nanocomposites, Int. J. Heat Mass Transf. 61 (2013) 577–582.
[11] C.W. Nan, R. Birringer, D.R. Clarke, H. Gleiter, Effective thermal conductivity of particulate composites with interfacial thermal resistance, J. Appl. Phys. 81 (10) (1997) 6692–6699.
[12] P.L. Kapitza, Heat transfer and superfluidity of helium II, Phys. Rev. 60 (4) (1941) 354.
[13] B. Riccardi, P. Fenici, A. Frias Rebelo, L. Giancarli, G. Le Marois, E. Philippe, Status of the European R&D activities on SiCf/SiC composites for fusion reactors, Fusion Eng. Des. 51 (2000) 11–22.
[14] T. Luo, J.R. Lloyd, Enhancement of thermal energy transport across graphene/graphite and polymer interfaces: a molecular dynamics study, Adv. Funct. Mater. 22 (12) (2012) 2495–2502.
[15] P.K. Schelling, S.R. Phillpot, P. Keblinski, Comparison of atomic-level simulation methods for computing thermal conductivity, Phys. Rev. B 65 (14) (2002) 144306.
[16] P.K. Schelling, S.R. Phillpot, P. Keblinski, Kapitza conductance and phonon scattering at grain boundaries by simulation, J. Appl. Phys. 95 (11) (2004) 6082–6091.
[17] F. Müller-Plathe, A simple nonequilibrium molecular dynamics method for calculating the thermal conductivity, J. Chem. Phys. 106 (1997) 6082.
[18] S. Plimpton, Fast parallel algorithms for short-range molecular dynamics, J. Comput. Phys. 117 (1) (1995) 1–19.
[19] C. Tang, L. Meng, H. Xiao, J. Zhong, Growth of graphene structure on 6H–SiC (0001): molecular dynamics simulation, J. Appl. Phys. 103 (2008) 063505.
[20] J. Tersoff, Modeling solid-state chemistry: interatomic potentials for multicomponent systems, Phys. Rev. B 39 (8) (1989) 5566–5568.
[21] J.F. Ziegler, J.P. Biersack, U. Littmark, The Stopping and Range of Ions in Solids, vol. 1, Pergamon Press, New York, 1985.
[22] S.J. Stuart, A.B. Tutein, J.A. Harrison, A reactive potential for hydrocarbons with intermolecular interactions, J. Chem. Phys. 112 (2000) 6472.
[23] E.T. Swartz, R.O. Pohl, Thermal boundary resistance, Rev. Mod. Phys. 61 (3) (1989) 605.
[24] M. Hu, D. Poulikakos, Graphene mediated thermal resistance reduction at strongly coupled interfaces, Int. J. Heat Mass Transf. 62 (2013) 205–213.
[25] R.E. Taylor, H. Groot, J. Ferrier, Thermophysical Properties of CVD SiC. TRPL1336, Thermophysical Properties Research Laboratory Report, School of Mechanical Engineering, Purdue University, 1993.
[26] C.A. Klein, M.G. Holland, Thermal conductivity of pyrolytic graphite at low temperatures. I. Turbostratic structures, Phys. Rev. 136 (2A) (1964) A575.
[27] A. Bagri, S.P. Kim, R.S. Ruoff, V.B. Shenoy, Thermal transport across twin grain boundaries in polycrystalline graphene from nonequilibrium molecular dynamics simulations, Nano Lett. 11 (9) (2011) 3917–3921.
[28] J.P. Crocombette, L. Gelebart, Multiscale modeling of the thermal conductivity of polycrystalline silicon carbide, J. Appl. Phys. 106 (8) (2009) 083520.
[29] G.E. Youngblood, D.J. Senor, R.H. Jones, S. Graham, The transverse thermal conductivity of 2D-SiCf/SiC composites, Compos. Sci. Technol. 62 (9) (2002) 1127–1139.
[30] R.J. Stevens, L.V. Zhigilei, P.M. Norris, Effects of temperature and disorder on thermal boundary conductance at solid–solid interfaces: nonequilibrium molecular dynamics simulations, Int. J. Heat Mass Transf. 50 (19) (2007) 3977–3989.
[31] A. Cao, J. Qu, Kapitza conductance of symmetric tilt grain boundaries in graphene, J. Appl. Phys. 111 (5) (2012). 053529–053529.
[32] Y. Katoh, L.L. Snead, T. Nozawa, S. Kondo, J.T. Busby, Thermophysical and mechanical properties of near-stoichiometric fiber CVI SiC/SiC composites after neutron irradiation at elevated temperatures, J. Nucl. Mater. 403 (1) (2010) 48–61.
[33] Y. Katoh, T. Nozawa, A.M. Williams, T. Cheng, P. Dou, L.L. Snead, Properties of Hi-Nicalon Type-S CVI SiC composite irradiated to 70 dpa at elevated temperatures, ORNL/TM-2012/459, Oak Ridge National Lab, 2012.
[34] J. Li, L. Porter, S. Yip, Atomistic modeling of finite-temperature properties of crystalline β-SiC: II. Thermal conductivity and effects of point defects, J. Nucl. Mater. 255 (2) (1998) 139–152.
[35] T. Bus, Fundamental properties of point defects and small clusters in 3C–SiC: a combined molecular dynamics and experimental study, in: Department of Nuclear Engineering, University of California, Berkeley, California, 2006.
[36] J.P. Crocombette, L. Proville, Thermal conductivity degradation induced by point defects in irradiated silicon carbide, Appl. Phys. Lett. 98 (19) (2011) 191905.
[37] M. Bockstedte, A. Mattausch, O. Pankratov, Ab initio study of the migration of intrinsic defects in 3C–SiC, Phys. Rev. B 68 (20) (2003) 205201.
[38] Y. Katoh, N. Hashimoto, S. Kondo, L.L. Snead, A. Kohyama, Microstructural development in cubic silicon carbide during irradiation at elevated temperatures, J. Nucl. Mater. 351 (1) (2006) 228–240.
[39] C.A. Ratsifaritana, P.G. Klemens, Scattering of phonons by vacancies, Int. J. Thermophys. 8 (6) (1987) 737–750.
[40] P.G. Klemens, D.F. Pedraza, Thermal conductivity of graphite in the basal plane, Carbon 32 (4) (1994) 735–741.